Thermal Science and Engineering Progress 61 (2025) 103500

Contents lists available at ScienceDirect

Thermal Science and Engineering Progress

journal homepage: www.elsevier.com/locate/tsep

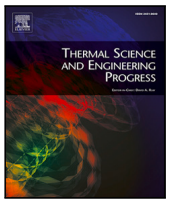

Cooling of a discrete heat source inside a horizontal channel linked with a composite open-cavity or protrusion

Amar S. Abdul-Zahra [a], Gazy F. Al-Sumaily [b,*], Hasanen M. Hussen [a], Mark C. Thompson [b], Hayder A. Dhahad [a]

[a] Mechanical Engineering Department, University of Technology, Iraq
[b] Department of Mechanical and Aerospace Engineering, Monash University, Clayton VIC 3800, Australia

ARTICLE INFO

Keywords:
Mixed convection
Channels
Cooling
Cavity
Protrusion

ABSTRACT

This study is a numerical investigation of the influence of using improved channel-cavity or channel-protrusion architectures on the augmentation of convection heat transfer and pressure drop. The effect of cavity depth $H_c \in [-1, 0]$ and protrusion height $H_c \in [0, 0.75]$ are investigated at various Reynolds number Re = 10, 40, 100 and Richardson number Ri = 0.1, 1, 5, 10. The governing equations are discretised and solved computationally employing the spectral-element method. The results show that the effect of the protrusion on the trend of Nusselt number is greater than the effect of the cavity. It is found that the existence of the cavity linked with the channel decreases substantially the heat transfer comparing with the smooth channel. However, the presence of the protrusion is found to increase significantly the heat transfer for all Reynolds and Richardson numbers. It is also found that in the channel-cavity flow, the pressure distribution along the channel is unaffected by the cavity height, excepting in the cavity zone. Nevertheless, the protrusion height increases significantly the pressure drop within the channel.

1. Introduction

Mixed convection, which incorporates simultaneously the effects of forced convection caused by a mechanical force and free convection caused by a temperature difference, is possible to be established in many electronic and telecommunication equipments such as air-cooling of integrated electronic circuit boards. Such systems include accumulating assemblage density that requires an efficient heat removal technique to assure acceptable performance. Many heat removal strategies have been recommended and their characteristics of heat transfer and fluid flow have been numerically and experimentally studied as elaborated by [1–5].

One of the commonly used strategies is by employing nano-fluids, in which the highly thermal conducting solid nano-additives are stably dispersed to the liquids and increase their viscosity and thermal conductivity, resulting in a higher heat removal, please see [6–15]. In addition, the geometry of a channel attached with an open enclosure or protrusion has been proposed as a new strategy that may achieve a high cooling effectiveness by considering more and active interaction between natural and forced convection flows due to the presence of the opening cavity or the protrusion on the surface of the channel. Fusegi [16] investigated unsteady mixed convective flow throughout a periodically grooved plate-channel. Thus, the lower channel plate is fluted at regular intervals to create multi open cavities, generating time-oscillatory flows, and the bottom cavity surface is heated by a constant heat flux. Their results showed that as Reynolds number and/or Womersley number increase, the main through-flow permeates further within each cavity, increasing the interaction between the main through-flow and the fluid inside the cavities. Consequently, this was found to considerably augment the heat dissipation from the warmed bottom surfaces of the cavities. [17,18] studied mixed convection heat dissipation inside a horizontal plate-channel containing an open cavity with the focus on the impact of the location of a local heat element positioned inside the cavity as well as on the cavity aspect ratio. They found that the position of the localised heater within the cavity significantly influences the interaction between the free convective flow produced in the cavity and the main forced flow inside the channel. For instance, Manca et al. [17] deemed three fundamental heating models for the open cavity: assisting flow, when the heat element is on the flow penetration side, opposing flow, when the heat element is opposite to the flow penetration side, and heating from the bottom surface of the

* Corresponding author.
E-mail addresses: amar.s.abdulzahra@uotechnology.edu.iq (A.S. Abdul-Zahra), gazy.alsumaily@monash.edu (G.F. Al-Sumaily), hasanen.m.hussen@uotechnology.edu.iq (H.M. Hussen), mark.thompson@monash.edu (M.C. Thompson), hayder.a.dhahad@uotechnology.edu.iq (H.A. Dhahad).

https://doi.org/10.1016/j.tsep.2025.103500
Received 4 October 2024; Received in revised form 7 March 2025; Accepted 8 March 2025
Available online 20 March 2025

Nomenclature

A	Amplitude of oscillatory flow.
f	Frequency of oscillatory flow, ($f = 1/\tau$).
H	Channel height, (m).
H_c	Cavity depth or protrusion height, (m).
L	Channel length, (m).
L_s	Length of heat source, (m).
Nu_m	Mean Nusselt number.
P	Non-dimensional pressure.
Pr	Prandtl number, $\mathrm{Pr} = c_p.\mu/k$.
Re	Reynolds number, $\mathrm{Re} = u_o.\rho.H/\mu$.
Ri	Richardson number, $\mathrm{Ri} = \mathrm{Gr}/\mathrm{Re}^2$.
T	Dimensional temperature, (°C).
t	Non-dimensional time.
u, v	Dimensional flow velocities, (m/s).
U, V	Non-dimensional group of velocities.
x, y	Dimensional Coordinates, (m).
X, Y	Non-dimensional coordinates.

Greek symbols

θ	Non-dimensional temperature.
μ	Fluid dynamic viscosity, (N s/m^2).
ρ	Fluid density, (kg/m^3).
τ	Time of one full period.

Subscripts

h	hot.
m	Mean.
n	Perpendicular.
o	Channel inlet.
out	Channel outlet.

cavity. They compared the thermal performance of these models and found that the opposing flow arrangement has the greatest thermal performance relating to both average Nusselt number and maximum temperature. Whereas, Aminossadati and Ghasemi [18] found that the heat transfer is improved significantly when changing the cavity aspect ratio for all different locations of the heat source. Brown and Lai [19] numerically examined heat and mass transfer from a horizontal plate-channel having an open shallow cavity located on the lower surface and heated from below. They performed a scale analysis and proposed correlations for mass-transfer driven air flows, that cover the whole convection regime, e.g., natural, mixed, and forced convection. Leong et al. [20] considered the same geometry utilised by Brown and Lai [19] to study mixed convection heat transfer for broad ranges of Reynolds and Grashof numbers as well as the cavity aspect ratio. It was found that Reynolds and Grashof numbers administer the appearance of recirculating cells, whereas the aspect ratio affects the direction of the cells. They reported that for a cavity having larger aspect ratio, the flow field might become unstable for high Grashof numbers and at a critical value of Reynolds number. Periodic and non-periodic oscillatory flows were observed. Manca et al. [21] carried out an experimental investigation on mixed convection inside an open cavity with a heated vertical wall on the inflow left side, bounded from the above by unheated horizontal plate. They presented results in terms of flow visualisation and temperature profiles on the heated wall for different height/width cavity ratios. They figured out that the larger the cavity width, the lower the wall temperature, and the higher the heat transfer. The flow visualisation showed that for high Reynolds number, a forced parallel flow in the main channel with a recirculating flow in the cavity are observed. Whereas, for low Reynolds number, there is a penetration of thermal plume from the vertical heated wall into the horizontal channel due to the strong impact of buoyancy forces. Sabbar et al. [22] studied numerically unsteady mixed convective airflow within a horizontal duct connected to an open cavity heated from below, with one or both vertical sides are made from elastic materials. They deduced that considering elastic walls for the cavity improves the rate of heat transfer compared to the rigid walls. Garcia et al. [23] studied unsteady mixed convective flow within an inclined channel with two identical facing open cavities exposed to discrete heating walls facing the opening. It was reported that depending on the aspect ratio of the cavity and the channel inclination, steady, periodic, quasi-periodic, and chaotic flow regimes were identified. Laouira et al. [24] examined the influence of the heat source length on mixed convection inside a channel with an open trapezoidal enclosure heated from the bottom. It was noted that the heat transfer increases with increasing the length of the heating element. Farhan et al. [25] investigated the impact of the heat source location on mixed convective flow and isotherm fields inside three channel-open cavity configurations. The results showed that with the heating elements' positions being changed, the velocity and pressure distributions seem to be unchanged throughout the channel. Firoozi et al. [26] conducted a numerical assessment to test the performance of passive techniques, namely dimples and nanofluids, on the convective heat transfer augmentation from dimpled tubes. They used Al2O3/Water nanofluid with various volume concentrations of nano particles in tubes with 27 variant dimple configurations. A Performance Evaluation Criteria (PEC) was employed to quantify the overall thermal-hydraulic improvement. The results showed that a maximum PEC value of 2.5 can be obtained using an optimal-designed dimpled tube. Whereas, a maximum PES value of 3.12 can be scored by using Al2O3/Water nanofluid with 4% volume friction.

Gazi et al. [27] investigated the heat transfer from a dimpled surface of a channel with and without protrusions on the opposite surface. Their results revealed that the protrusions increase the shedding of vortical secondary flow structures induced by the dimples. Consequently, considerable augmentations in heat transfer with greater Reynolds number dependence are resulted in comparing to the case of a channel with smooth upper surface and dimples on one opposite surface. Yonghui et al. [28] investigated the effects of using dimples and protrusions on the heat transfer performance and mixed convective nano-fluid flow, covering laminar, transitional, and turbulent regimes within a rectangular channel. The results revealed that the employment of protrusions and dimples greatly enhances the performance of heat transfer. It was found that the influence of dimple-case has the significant difference with that of protrusion-case. It was recommended to use the protrusions under laminar flow for its superior heat transfer augmentation; however, to adopt the dimples under turbulent flow to avoid excessive friction and high pumping power. Sahu et al. [29] tested the influence of right-angle triangular protrusions on the lower surface of a horizontal channel on the thermal-hydraulic performance. They found that more rates of heat transfer can be gained at larger protrusion pitch, and lower pressure drop is occurred in case of smaller height of protrusion. Sobhani and Behzadmehr [30] examined the effect of different shapes of dimples and protrusions on the thermo-fluid flow conduct within a horizontal tube for finding an appropriate configuration for which heat transfer and pressure drop to be counterbalanced. They indicated that in general, the augmentation in heat transfer is more than the cost of pumping power. Thus, the results showed that employing improved tube duplicates the heat transfer, whereas the friction coefficient is increased by 25%. For the configuration of channel-protrusion assembly, Ebubekir et al. [31] investigated how the flow field and the heat transfer are impacted by the presence of triangular guide protrusions mounted on the upper surface of a channel, within forced convective laminar flow conditions. It was found that the existence of protrusions changes completely the flow patterns, including the speed of the axial core flow and the recirculating flow

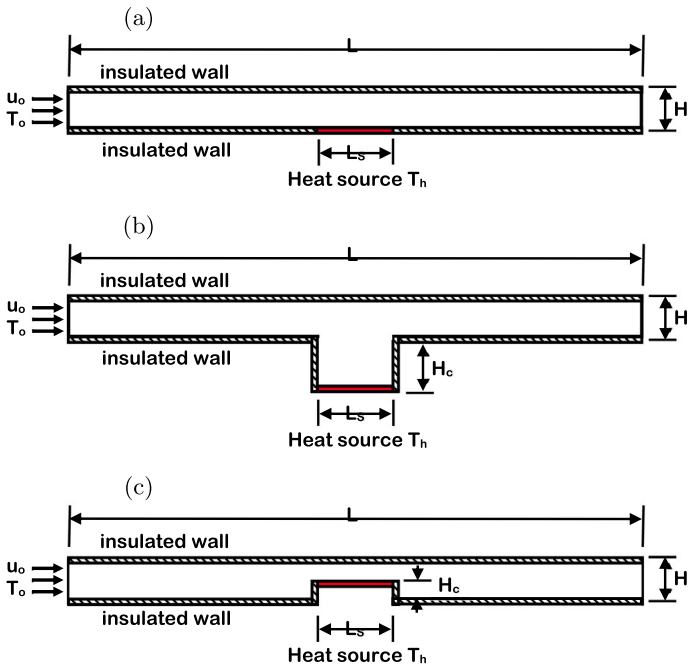

Fig. 1. Physical configurations deemed in the present study, (a) Flat channel, (b) Channel with cavity, (c) Channel with protuberance.

between the blocks, resulting in a significant change in the transporting thermal energy. Shaik et al. [32] studied the enhancement of thermal performance of solar air heaters by using protrusions in their absorber plates. A significant heat transfer augmentation of 101% was observed in the modified air heater with protrusions.

By inspection of the aforementioned literature review, it can be seen that dimples and protrusions have been used as good forms of passive cooling methods, which have the great capacity of heat transfer augmentation without too much flow resistance penalty. However, only Yonghui et al. [28] compared their effects on the mixed convective flow and heat transfer performance, and discovered that there is a significant difference between the dimple-case and the protrusion-case. As such, the objective of this research is to study the heat transfer performance and pressure drop characteristic of laminar mixed convective air-flow in a conventional horizontal plate-channel with an open-cavity or protrusion containing a heat source on its entire horizontal lower surface, with the emphasis on the influence of cavity depth and protrusion height. This will provide a worthy assessment on which kind of these technique is an adequate design resulting in superior cooling performance in high-heat generating electronic devices.

2. Mathematical formulation

The geometry considered in the present study is illustrated in Fig. 1. Air is introduced to the channel from the left opening at a uniform inlet velocity (u_o) and temperature (T_o). The walls of the channel and the cavity or the protrusion are insulated, except its bottom surface, which is assumed to be isothermally heated at temperature (T_h). The channel height is (H), and the channel length is assumed to be long enough ($L = 11H$) to avoid the channel ends' effects. The length of heat source is assumed to be equal to the channel height ($L_s = H$), and is located in the middle of the lower surface of the channel. The cavity depth or the protrusion height (H_c) is variable within the study. In this numerical investigation, the channel height is used as a characteristic length scale and considered to be equal to unity ($H = 1$), to simplifying the non-dimensionalisation and scaling process of the governing equations.

The simplifying assumptions employed in the current study are as follows:

1. The flow is two-dimensional, Newtonian, unsteady, incompressible and laminar with Prandtl number of Pr = 0.71.
2. The heat generation and Radiation are ignored.
3. The thermo-physical properties of the air are maintained invariable, except the density, and the approximation of Boussinesq is used to calculate its linear dependency on the temperature by the following approximation:

$$\rho = \rho_o[1 - \beta(T - T_o)], \tag{1}$$

where (β) is the coefficient of thermal expansion, which is calculated as follows:

$$\beta = -\frac{1}{\rho_o}\left(\frac{\partial \rho}{\partial T}\right)_P. \tag{2}$$

Accordingly, the dimensionless format of the governing equations for the existent physical model can be expressed as follows (Al-Sumaily et al. [33], Dhahad et al. [34], Al-Sumaily et al. [35]):

$$\left(\frac{\partial U}{\partial X} + \frac{\partial V}{\partial Y}\right) = 0, \tag{3}$$

$$\frac{\partial U}{\partial t} + \left(U\frac{\partial U}{\partial X} + V\frac{\partial U}{\partial Y}\right) = -\frac{\partial P}{\partial X} + \frac{1}{\mathrm{Re}}\left(\frac{\partial^2 U}{\partial X^2} + \frac{\partial^2 U}{\partial Y^2}\right), \tag{4}$$

$$\frac{\partial V}{\partial t} + \left(U\frac{\partial V}{\partial X} + V\frac{\partial V}{\partial Y}\right) = -\frac{\partial P}{\partial Y} + \frac{1}{\mathrm{Re}}\left(\frac{\partial^2 V}{\partial X^2} + \frac{\partial^2 V}{\partial Y^2}\right) + \mathrm{Ri}\ \theta, \tag{5}$$

$$\frac{\partial \theta}{\partial t} + \left(U\frac{\partial \theta}{\partial X} + V\frac{\partial \theta}{\partial Y}\right) = \frac{1}{\mathrm{Re.Pr}}\left(\frac{\partial^2 \theta}{\partial X^2} + \frac{\partial^2 \theta}{\partial Y^2}\right), \tag{6}$$

where (X) and (Y) are the dimensionless Cartesian coordinates; (U) and (V) are the dimensionless horizontal and vertical velocities; (P) and (t) are the dimensionless pressure and time; and (θ) is the dimensionless temperature. The following characteristic scaling variables are used to produce the dimensionless equations:

$$U = \frac{u}{u_o},\ V = \frac{v}{u_o},\ X = \frac{x}{H},\ Y = \frac{y}{H},\ P = \frac{p}{\rho u_o^2},\ t = \frac{t'}{u_o H},\ \theta = \frac{(T - T_o)}{(T_H - T_o)}, \tag{7}$$

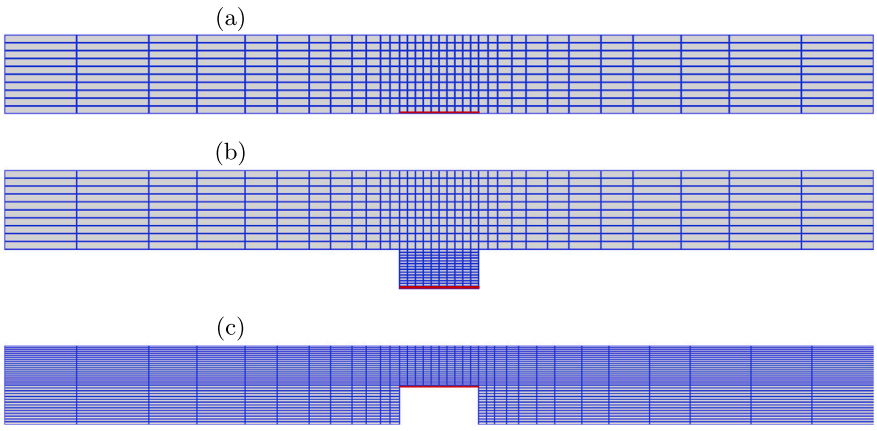

Fig. 2. Computational meshes deemed in the present study, (a) Flat channel, (b) Channel with cavity $H = -0.5$, (c) Channel with protuberance $H = 0.5$.

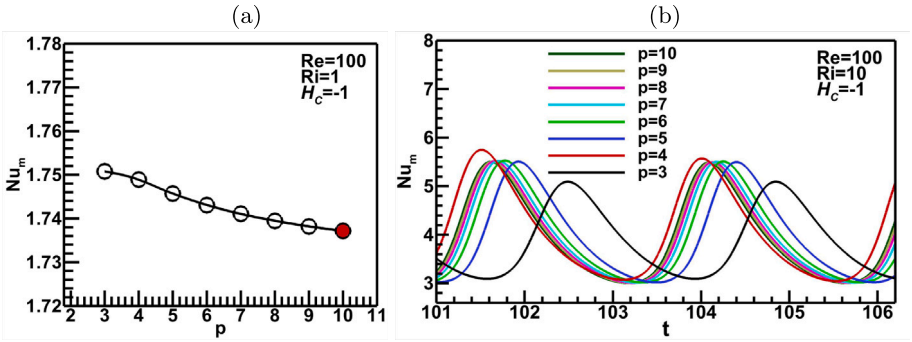

Fig. 3. Mesh resolution analysis; (a) Nu_m against p, and (b) the temporal variation of Nu_m showing the oscillatory behaviour.

where (x) and (y) are the dimensional Cartesian coordinates; (u) and (v) are the dimensional horizontal and vertical velocities; (p) and (t') are the dimensional pressure and time; and (T) is the dimensional temperature. The primary dimensionless applicable parameters that might be interesting for such sort of fluid flow are Reynolds number (Re), Richardson number (Ri), and Prandtl number (Pr), which perhaps described as:

$$\mathrm{Re} = \frac{u_o \rho H}{\mu},\ \mathrm{Ri} = \frac{\mathrm{Gr}}{\mathrm{Re}^2},\ \mathrm{Gr} = \frac{g.\beta.\rho^2.H^3(T_h - T_o)}{\mu^2},\ \mathrm{Pr} = \frac{c_p.\mu}{k}, \tag{8}$$

here, (Gr) is Grashof number, (μ), (ρ), (k) are the viscosity, density, and thermal conductivity of the flowing fluid, respectively.

The rate of heat exchange between the horizontal heat element and the adjacent cooling fluid is calculated by means of a non-dimensional quantity namely, the mean Nusselt number (Nu_m), as follows:

$$\mathrm{Nu}_m = \frac{1}{L_s}\int_0^{L_s}(-\frac{\partial\theta}{\partial n}).dX, \tag{9}$$

where (n) is the normal length on the heat element.

3. Numerical procedure

The highly connected non-dimensional governing Eqs. (3)–(6) are discretised computationally in space and time. The spectral-element method, which is similar to the finite element method, is used for the space integration, while the classic splitting scheme, suggested by Chorin [37] and detailed in Karniadakis et al. [38], is used for the time integration. In the spatial discretisation, the computational domain is initially divided into a macro-mesh of individual elements. Within the numerical run, a high-order polynomial (p) basis over each element can be used, allowing swift convergence with raising the degree of the polynomial (Karniadakis et al. [38]). The elemental mesh is condensed in regions of the computational domain that undergo high velocity gradients. The macro-meshes depicting the spatial discretisation of the computational domains deemed in the present study, e.g. flat channel, channel with a cavity, and channel with a protuberance, are illustrated Fig. 2. In the temporal discretisation, the nonlinear advection terms of the momentum and energy Eqs. (4)–(6) are integrated in the first step, and then the step calculating for the impact of the pressure gradient is performed, and the diffusion terms are integrated in the final step.

To numerically solve the current physical problem, the dimensionless initial and boundary conditions should be first mathematically assigned. First, the velocity and temperature fields are set initially to zero, $(U = V = \theta = 0)$, at $(t = 0)$ over the entire computational domain. Then, for $(t > 0)$: the boundary conditions are set as follows: Along the inlet opening, at ($X = 0$ and $Y = 0$ - H), a uniform inlet horizontal flow with velocity components ($U_o = 1$ and $V_o = 0$) are implemented, with a temperature set to zero ($\theta_o = 0$) as a cooling fluid. Along the outlet opening, at (X = L and $Y = 0$ - H), the normal gradient condition set to zero is implemented for velocities and temperature ($\partial U/\partial X = \partial V/\partial X = \partial\theta/\partial X = 0$). On the heating element, at ($Y = 0$ and X = along L_s), a constant temperature ($\theta_h = 1$) condition is enforced with no-slip

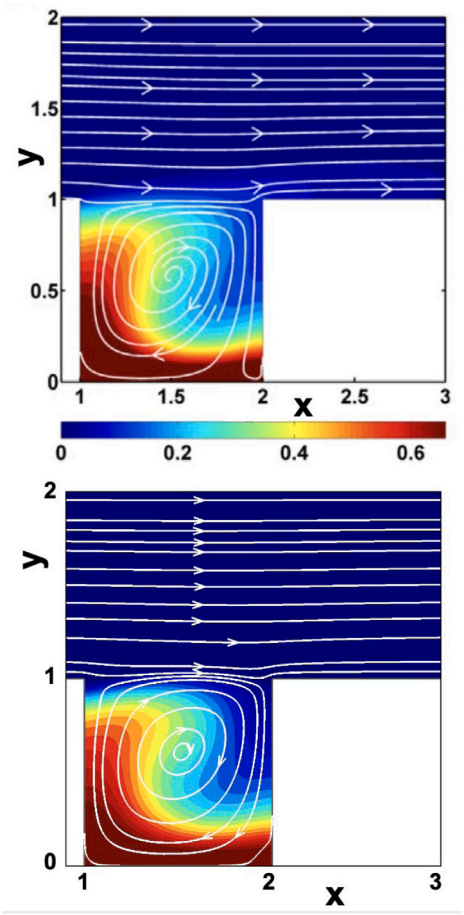

Fig. 4. Comparison between the results of Abdelmassih et al. [36] (Top) and our code (Bottom).

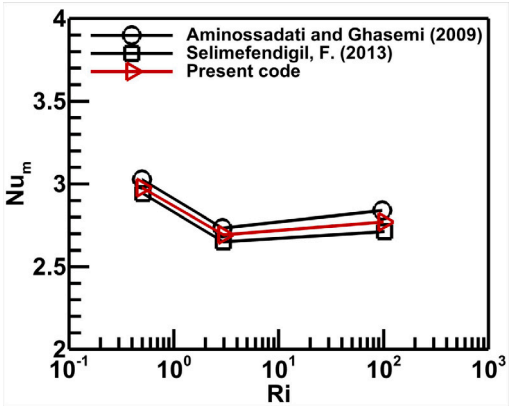

Fig. 5. Comparison amongst the results of Aminossadati and Ghasemi [18], Selimefendigil [39], and the present solver.

condition ($U = V = 0$). The other solid boundaries of the channel are assumed to be insulated ($\partial\theta/\partial Y = 0$) and no-slippery ($U = V = 0$).

The computational meshes shown in Fig. 2 were tested by a convergence analysis for choosing adequate spatial resolution to ensure that the calculational results are grid-independent. This analysis was conducted by changing the element polynomial order p from 3 to 10, while holding the macro-elemental allocation unaltered. The mean Nusselt number Nu_m was monitored to check its sensitivity to the spatial resolution. The convergence test was carried out for different values of Reynolds number Re, Richardson number Ri, and cavity/protrusion depth H_c. The results showed that the convergence with differences less than %0.1 can be obtained with polynomial order of p = 10, which is later employed for all simulations of the present study. Samples of the results of the convergence tests are presented in Fig. 3 for the case of an oscillatory flow in a channel with heated cavity having a depth of $H_c = -1$, at Re = 100 and Ri = 1.

The numerical code was validated multiple times against published results for flow, temperature, and heat transfer to ascertain the precision of its existing algorithm. Fig. 4 demonstrates a qualitative comparison between the results of the present code and the numerical results of Abdelmassih et al. [36] for streamline and isotherm patterns within a cavity linked with a horizontal channel, and heated entirely from the bottom, and having a depth of $H_c = -1$, at Re = 100 and Ri = 1. Whereas, Fig. 5 depicts a quantitative comparison for the results of mean Nusselt number calculated by the present solver and those published by Aminossadati and Ghasemi [18] and Selimefendigil [39] for the case of mixed convection heat transfer from a discrete heater installed on the bottom surface of a cavity opened to a horizontal channel for ($Ri = Gr/Re^2$) ranging between 0.5 and 100. It can be seen that very good agreements with published results are found.

4. Results and discussion

In the current study, characteristics of air-flow (Pr = 0.71), temperature distribution, and heat transfer of mixed convection inside a horizontal channel connected on the bottom surface with either open cavity or protrusion, are investigated. The emphasis is to study the effect of cavity depth or protrusion height H_c (from −1 to 0 for cavity, and from 0 to 0.75 for protrusion, with an interval of 0.25), at different Reynolds and Richardson numbers, i.e., Re = 10, 40, 100 and Ri = 0.1, 1, 5, 10, respectively.

Figures 6–8 demonstrate the effect of varying the cavity depth and the protrusion height (containing the heat source) on the flow conduct and temperature distribution inside the channel for Re = 10, 40, 100 and at Ri = 1, while Figs. 9–11 illustrate this effect for same Reynolds numbers, but at Ri = 10. The figures show that in the cavity case, the cavity allows for air to enter throughout its centre and then expels it outward from the opposite wall. Also, the increase in the cavity depth leads to increasing the flow recirculation inside the cavity and above the heat source. Whereas, in the protrusion case, the increase in the protrusion height increases the flow velocity above the heat source due to the area contraction. This induces an increase in the intensity of flow recirculation in the area behind the protrusion (after the heat source) and towards the downstream of the channel. Based on the results, it is observed that as Reynolds number or Richardson number increases, the intensity of recirculating flow inside the cavity or after the protrusion increases, resulting in a more effective cooling effect for all instances. For example, at Ri = 1, $H_c = -0.5$, and Re = 10 as in Fig. 6, the cavity permits air to flow in throughout its inner surface and exit out from the opposite wall with creating only small eddies in the cavity corners. Whereas, at Re = 40 as in Fig. 7, a single vortex is generated occupying the entire cavity. In addition, interestingly, Fig. 11 depicts that at the deepest cavity at $H_c = -1$ and higher Reynolds number Re = 100, two distinct vortexes are produced within the cavity, which may produce thermal cavity region with low temperature gradients, leading to a decrease in the heat convection.

As opposed to that, the plots show that the temperature distribution patterns inside the cavity are hardly altered, resulting in a high temperature region above the heat source. However, it is quite obvious that the high temperature levels in this region remarkably decreases in the

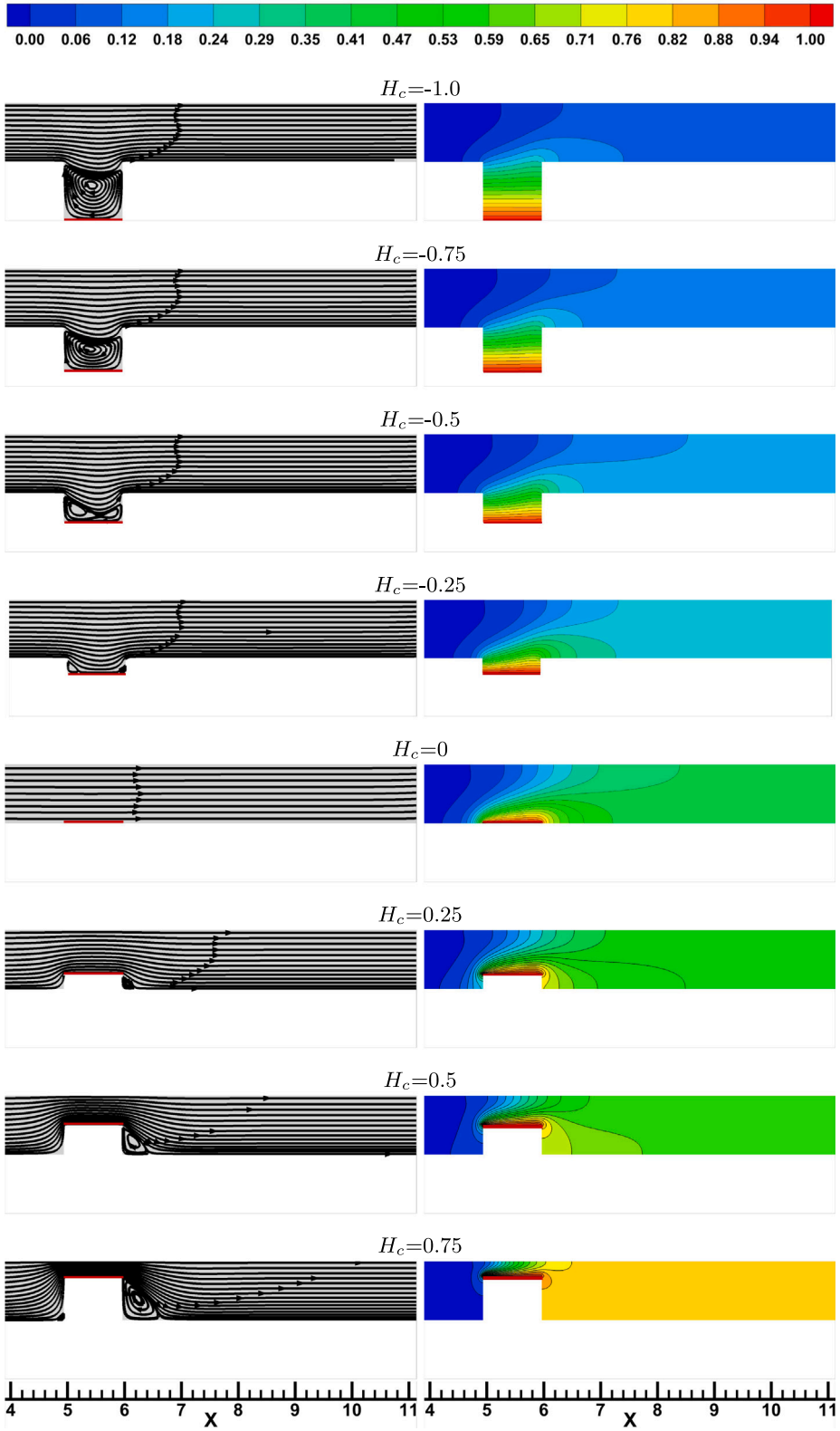

Fig. 6. Zooming for (Left) Streamlines patterns and (Right) isotherms patterns, at different heights of heat source and at Re = 10, and Ri = 1.

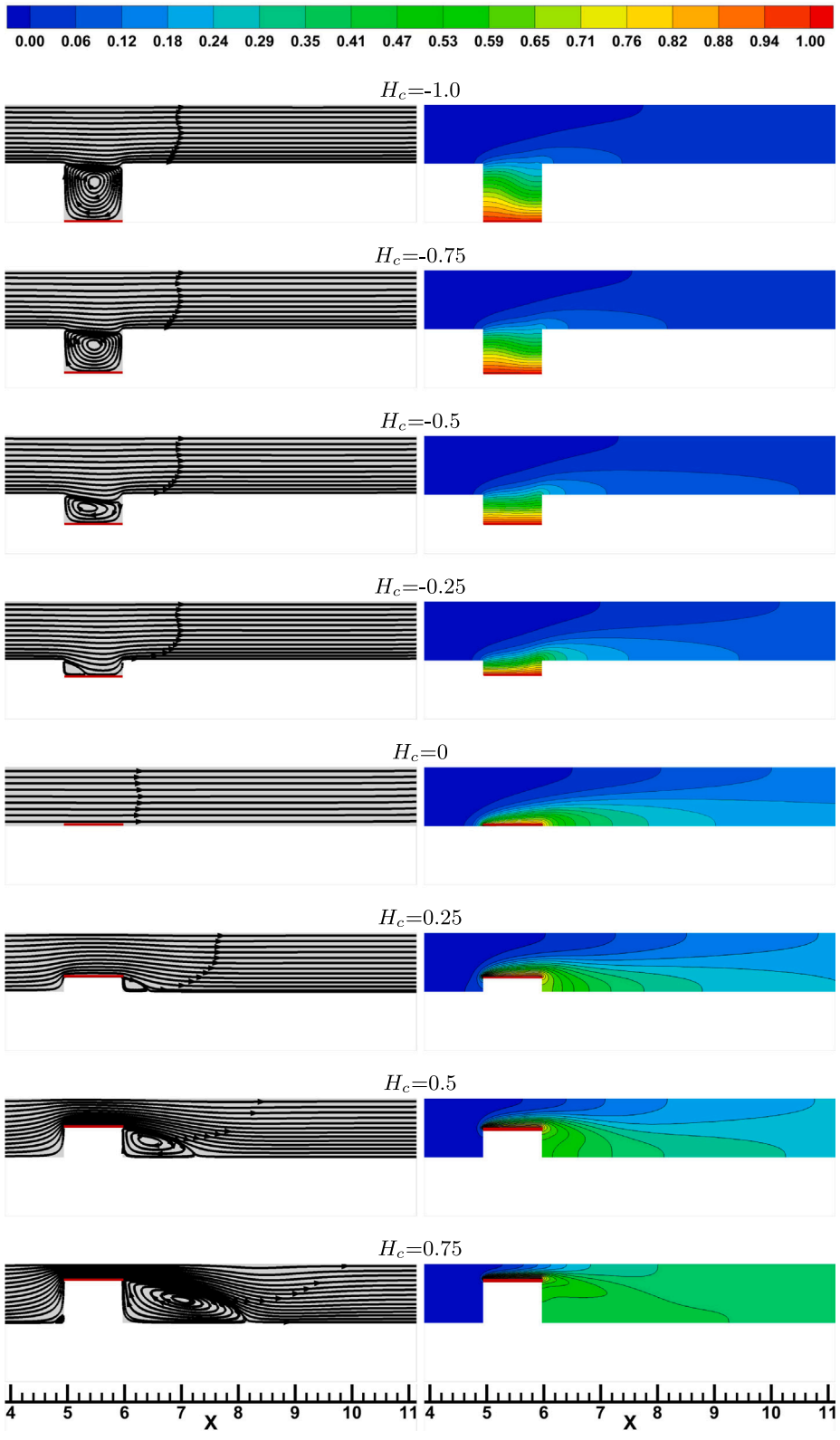

Fig. 7. Zooming for (Left) Streamlines patterns and (Right) isotherms patterns, at different heights of heat source and at Re = 40, and Ri = 1.

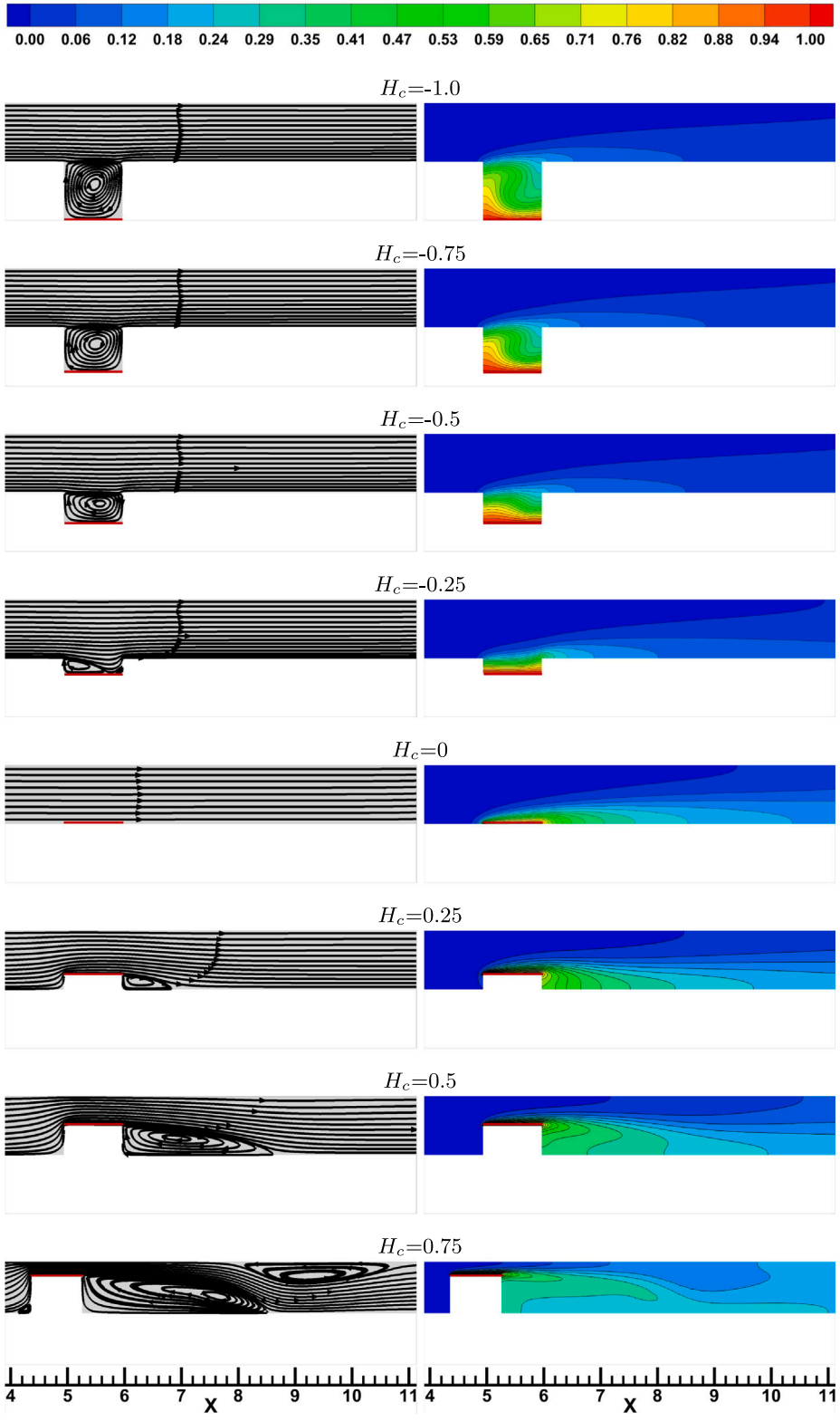

Fig. 8. Zooming for (Left) Streamlines patterns and (Right) isotherms patterns, at different heights of heat source and at Re = 100, and Ri = 1.

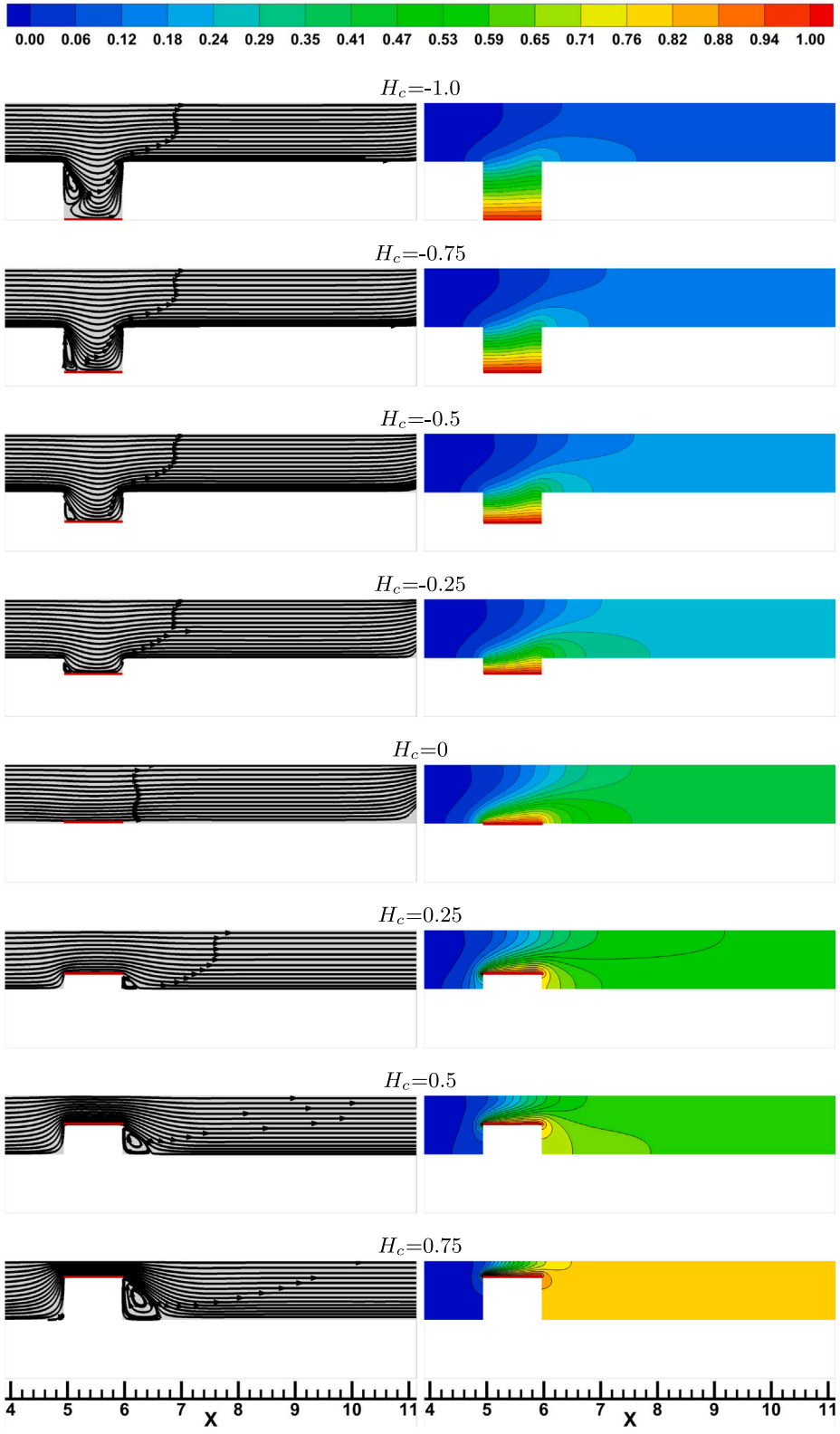

Fig. 9. Zooming for (Left) Streamlines patterns and (Right) isotherms patterns, at different heights of heat source and at Re = 10, and Ri = 10.

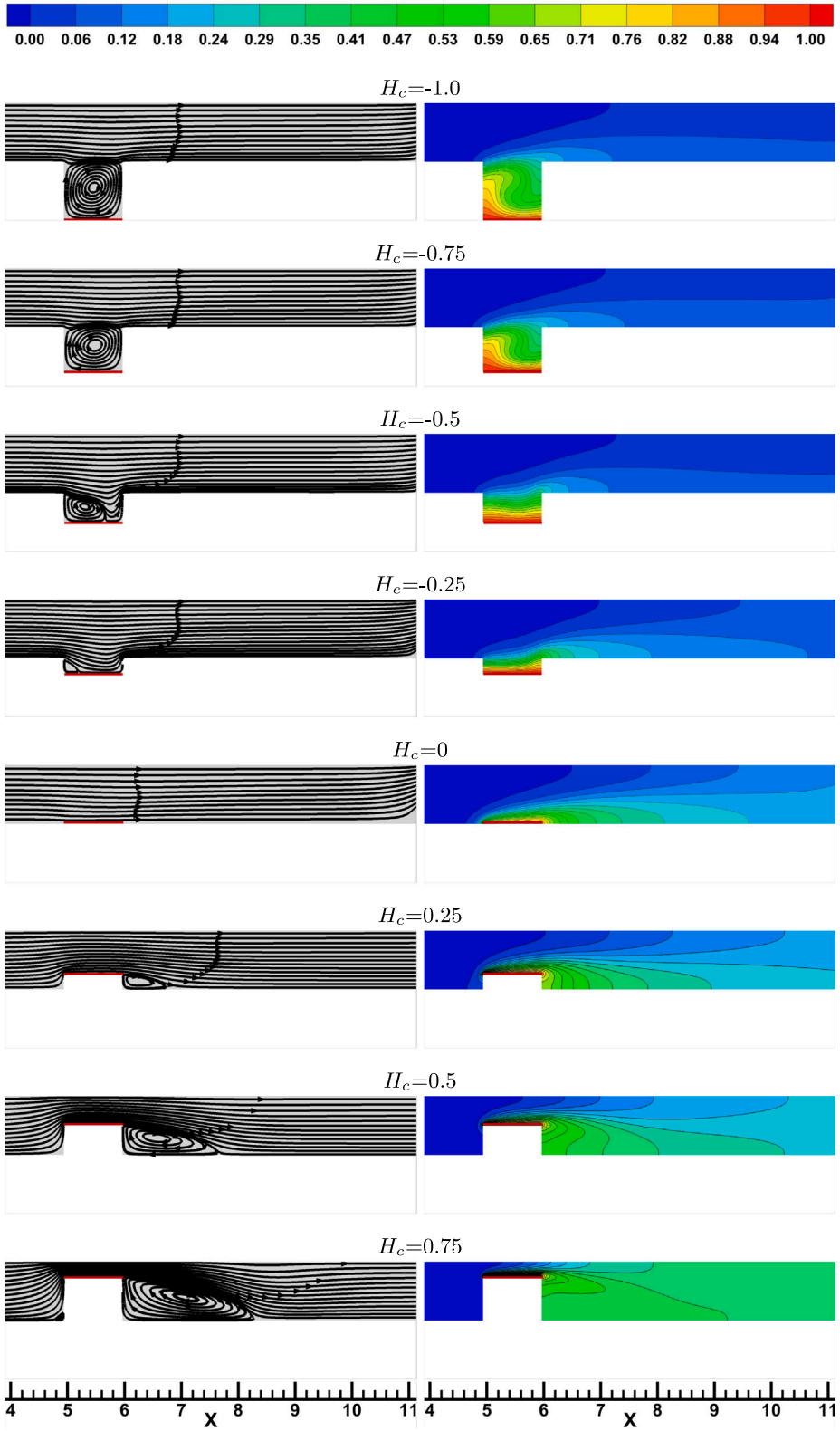

Fig. 10. Zooming for (Left) Streamlines patterns and (Right) isotherms patterns, at different heights of heat source and at Re = 40, and Ri = 10.

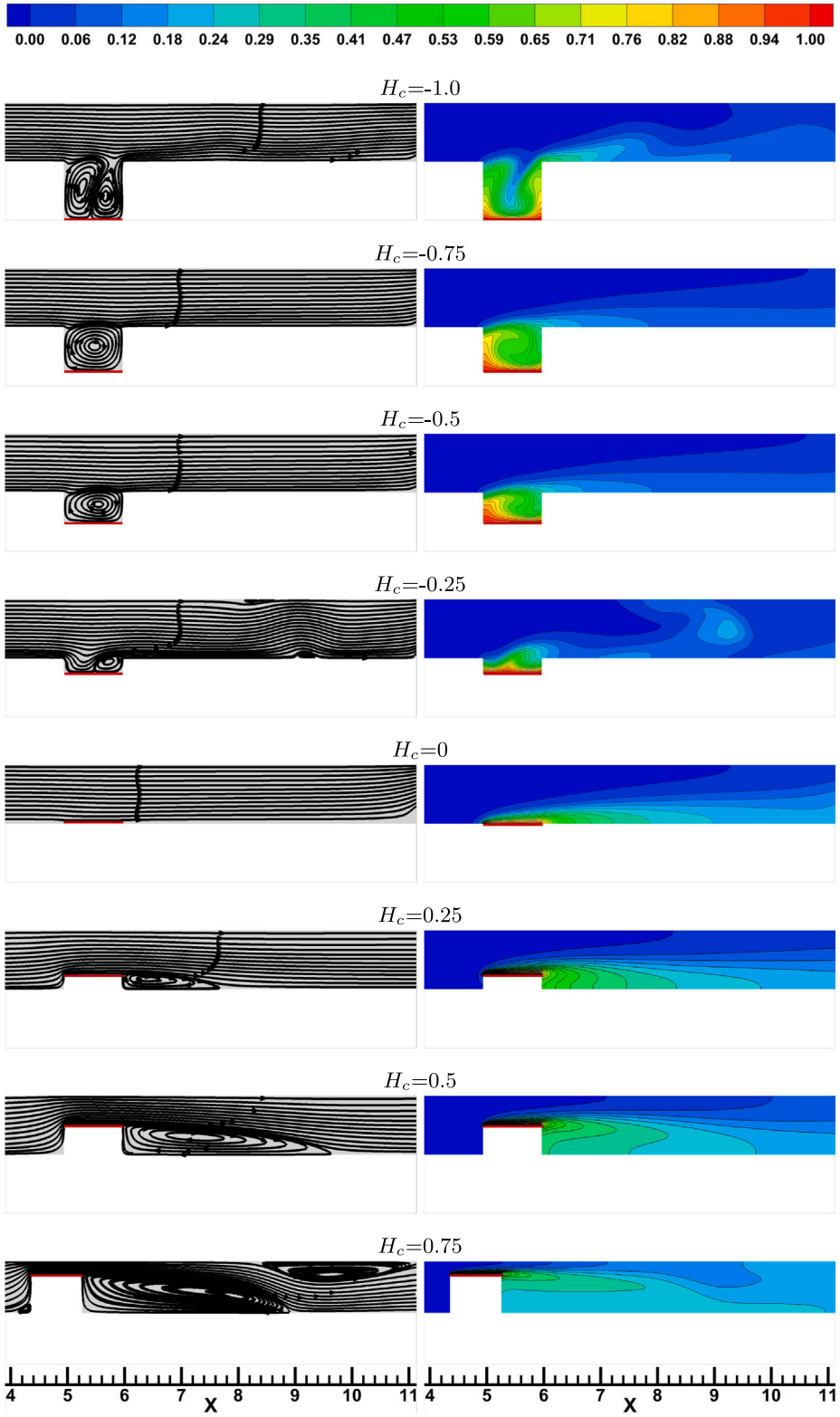

Fig. 11. Zooming for (Left) Streamlines patterns and (Right) isotherms patterns, at different heights of heat source and at Re = 100, and Ri = 10.

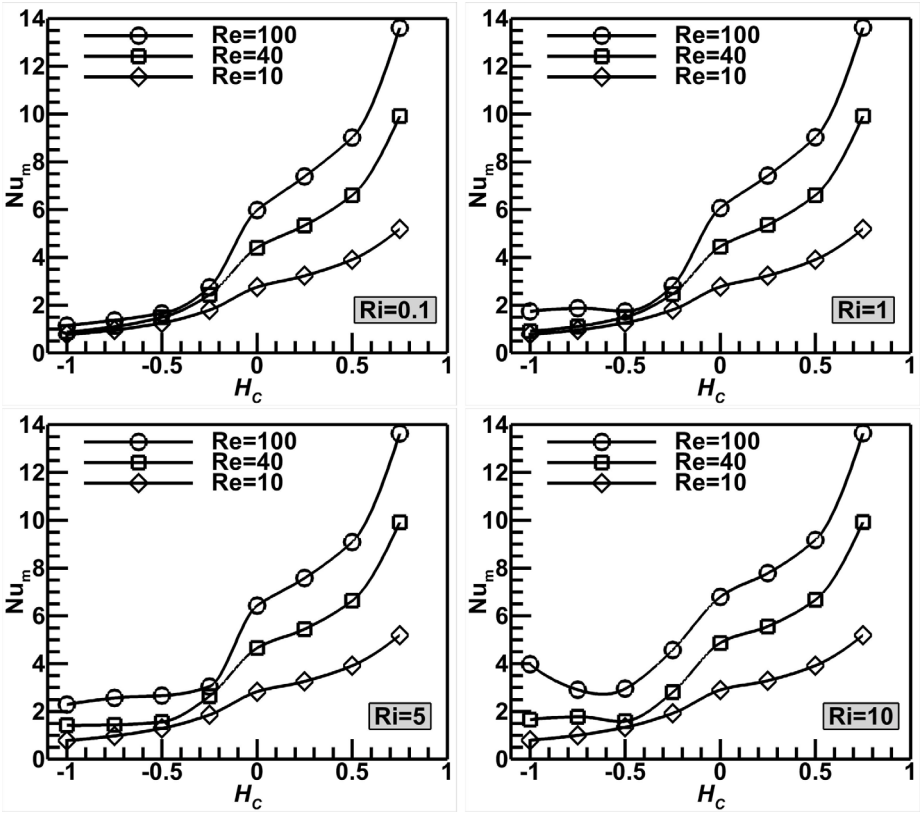

Fig. 12. Variation of mean Nusselt number against cavity depths and protrusion heights at different Reynolds and Richardson numbers.

protrusion-case, indicating the great augmentation of convection heat transfer. Moreover, the whole temperature level prominently reduce when increasing Reynolds number.

Fig. 12 displays the impact of the depth of cavity $H_c \in [-1, 0]$ and the height of the protrusion $H_c \in [0, 0.75]$ on the average Nusselt number (Nu_m), at $\mathrm{Re} = 10, 40, 100$ and $\mathrm{Ri} = 0.1, 1, 5, 10$. For all cases, the plots demonstrate that the effect of the protrusion case on the trend of Nusselt number is much higher than the effect of the cavity case. Thus, for the cavity case, at low Richardson number $\mathrm{Ri} = 0.1$, it is shown that as the cavity depth increases, Nusselt number slightly increases for all Reynolds numbers. While, at $\mathrm{Ri} = 1$ and 5, it is seen that the effect of the cavity depth becomes trivial. However, at $\mathrm{Ri} = 10$, the trend of Nusselt number changes from slight positive into slight negative for Reynolds numbers $\mathrm{Re} = 40$ and 100. Indeed, this is attributed to the change in the flow from steady into unsteady status and generating multi-recirculating flow zones, and generating low temperature gradient thermal region inside the cavity. On the other hand, for the protrusion case, it can be seen that Nusselt number increases significantly with increasing the protrusion height for all circumstances of Reynolds and Richardson numbers. Furthermore, the influence of Reynolds number on Nusselt number in the cavity is minimal at $\mathrm{Ri} = 0.1$, and becomes considerable as Richardson number increases. Nevertheless, in the protrusion case, the influence of Reynolds number is robust and leading to higher values of Nusselt number at higher protrusion heights. That is due to the high air velocities in the vicinity of heat source in the compressed area.

Figs. 13–15 illustrate the pressure streamline contours for different channel-cavity and channel-protrusion flow assemblies at three cases of Reynolds numbers of ($\mathrm{Re} = 10, 40, 100$) and at a particular heating case of $\mathrm{Ri} = 1$. The graphics clearly show the growing of recirculating zones in the channel as changing the depth/height of cavity/protrusion. It can be seen that the pressure is higher at the inlet region of the channel, drops gradually as it travels, and changes at the positions where the cavity/protrusion and the channel meet. In the channel-cavity flow assembly, the pressure distribution through the channel is not impacted by the rise of the cavity height, except for the zone inside the cavity. Importantly, the same overall pressure difference is generated along the channel as the cavity depth is altered. Nevertheless, increasing the protrusion height causes a significant increase in the pressure difference within the channel.

Fig. 16 shows the variations of the percent of heat transfer enhancement (%HTE) and the pressure drop (%ΔP) for modified channels compared with the smooth channel, which are calculated as follows:

$$\%\mathrm{HTE} = \frac{\mathrm{Nu}_{m.modified} - \mathrm{Nu}_{m.smooth}}{\mathrm{Nu}_{m.modified}} \times 100\%, \tag{10}$$

$$\%\Delta\mathrm{P} = \frac{\Delta\mathrm{P}_{modified} - \Delta\mathrm{P}_{smooth}}{\Delta\mathrm{P}_{modified}} \times 100\%. \tag{11}$$

and the dimensional pressure drop (ΔP) is rescaled using the following equation:

$$\Delta\mathrm{P} = \left|\rho u_o^2 L\left(P_{out} - P_o\right)\right|. \tag{12}$$

Interestingly, the figure clearly shows that the presence of the cavity connected with the channel reduces significantly the heat transfer from the heat source compared to the smooth channel. It can be seen that as the cavity depth increases, the heat transfer augmentation decreases largely, and this negative effect becomes more pronounced at higher Reynolds numbers. Indeed, the flow boundary layer affects the near wall thermal boundary layer and increases or decreases the convective heat transfer coefficient. Thus, the negative influence of cavity depth can be attributed to the forming of two symmetrical large vortices occurring inside the cavity as the cavity depth increases, leading to

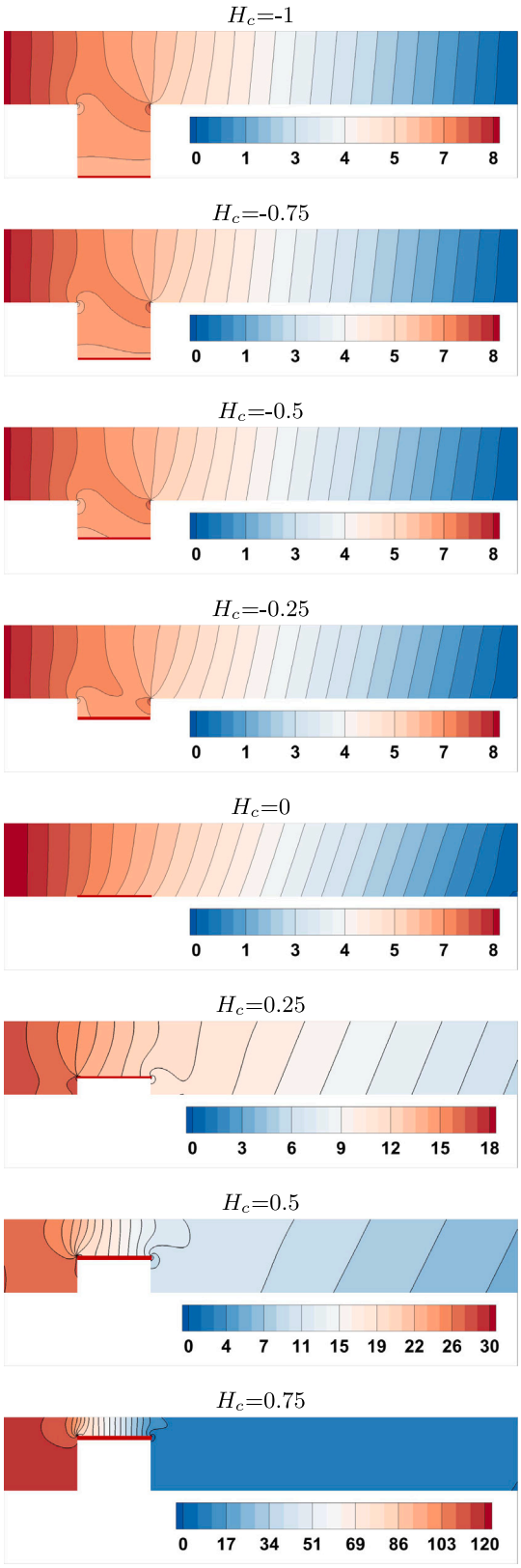

Fig. 13. Patterns of non-dimensional pressure distribution within the channel with different cavity depths and protrusion heights, at Re = 10, and Ri = 1.

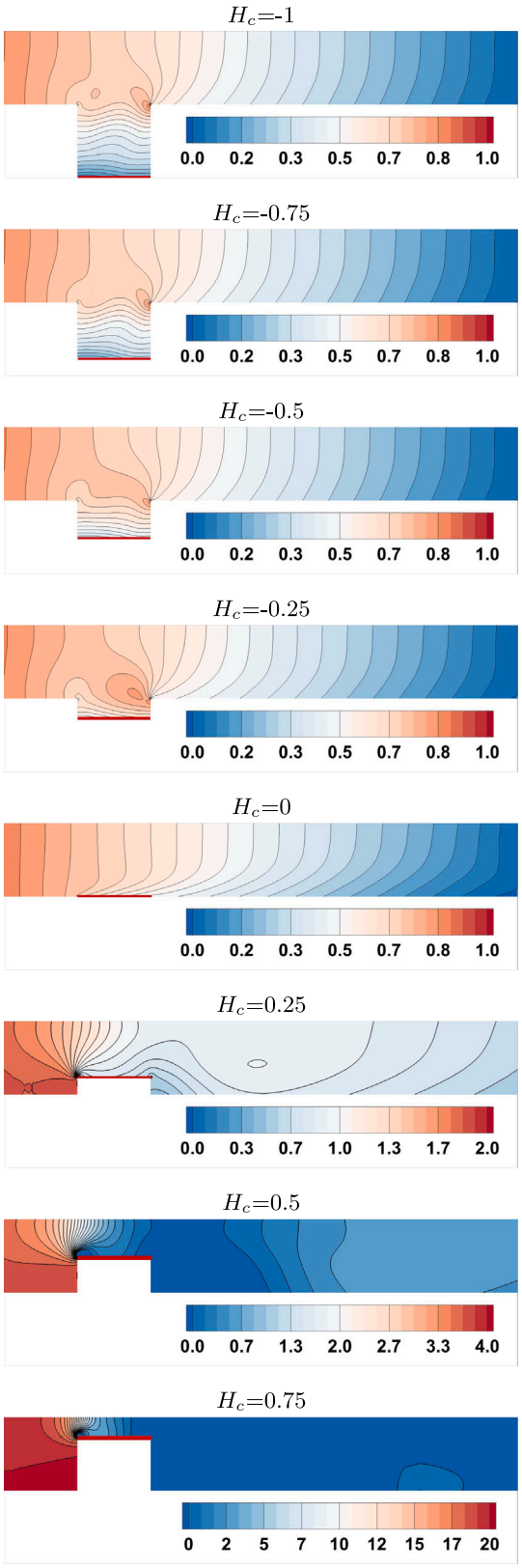

Fig. 14. Patterns of non-dimensional pressure distribution within the channel with different cavity depths and protrusion heights, at Re = 40, and Ri = 1.

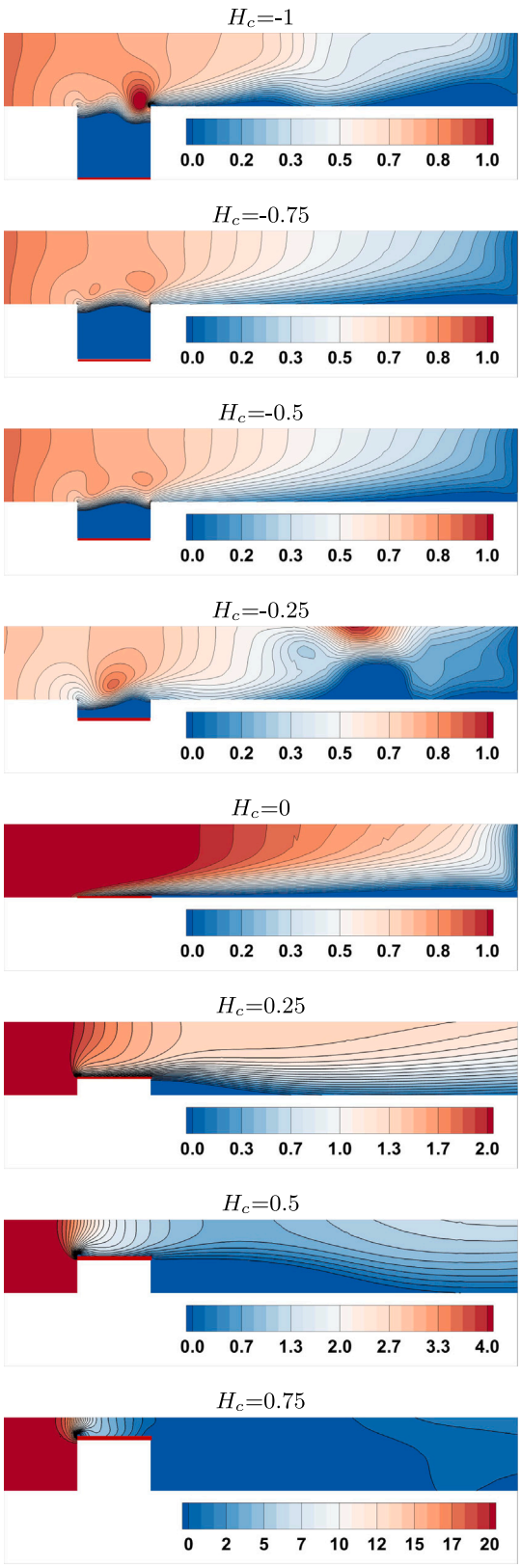

Fig. 15. Patterns of non-dimensional pressure distribution within the channel with different cavity depths and protrusion heights, at Re = 100, and Ri = 1.

two symmetrical high temperature regions. In addition, it is shown that the negative impact of the higher cavity depth is decreased at higher Richardson and Reynolds numbers. This may be due to changing in the flow behaviour in the cavity from two steady symmetrical eddies into unsteady periodically moving eddies. Whereas, the protrusion-case has an enormous benefit in increasing the heat transfer enhancement. However, the protrusion-case suffers from penalty of distinct friction increase due to increasing the pressure drop in the channel as the protrusion height increases.

Figures 17–19 demonstrate the temporal variation of Nusselt number measured above the heat source, for all values of the cavity depths or the protrusion heights, and for the circumstances when the fluid-flow inside the channel changes from steady into unsteady (periodic) condition or contrariwise such as at (Re = 40 and Ri = 10), (Re = 100 and Ri = 5), and (Re = 100 and Ri = 10). First of all, it is obvious that the transition in the fluid-flow occurs only in the case of a channel linked with a cavity (inside the cavity containing the heat source). However, the figures do not show that such transition is occurred in the case of a channel with a protrusion. It may happen in the channel-area that is behind the protrusion, but it is not measured by the temporal Nusselt number. Second, occurring the periodic flow in the cavity at a certain depth is not consistent. However, it depends on distinct parameters such as the strength of upcoming fluid-flow represented by Reynolds number, the degree of heating represented by Richardson number, and the cavity depth. For instance, it is seen that the fluid is undergoing unsteady periodic flow inside the cavity with a depth equals to ($H_c = -0.5$) for both conditions: When (Re = 40 and Ri = 10, as in Fig. 17 and when (Re = 100 and Ri = 5, as in Fig. 18. However, when (Re = 100 and Ri = 10), the unsteady flow is not appeared at the cavity depth of ($H_c = -0.5$), but interestingly it appears at ($H_c = -0.25$ and -1, as in Fig. 19).

It is important to investigate the conduct of periodic flows inside the cavity. Therefore, for each periodic-flow case, the period length is assigned, the flow oscillation frequency ($f = 1/\tau$), where (τ) is the time of one full period, and the oscillation amplitude (A) are measured. Also, many images describing the flow and thermal behaviours at different times over the single-period are captured and presented as streamlines and thermal contours, respectively, in Figures 20–23. In the figures, in a general sense, it can be observed that the oscillation frequency and amplitude are strongly positively influenced by Reynolds number, Richardson number, and/or the cavity depth. In Figs. 20 and 21, in these two cases, Richardson number is constant at Ri = 10, whereas Reynolds number increases from Re = 40 to 100, and the cavity depth decreases from $H = -0.5$ to -0.25. In Fig. 20, there is a single moderate flow-cell produced inside the cavity by the buoyancy effects referring to the dominance of free convection. The size of the single cell slightly expands and shrinks with the time producing a moderate flow fluctuating having oscillation frequency $f = 0.1649$ and amplitude $A = 0.0451$. However, in Fig. 21, as Reynolds number increases, the pressure forces attempt to suppress the recirculating vortex, and the buoyancy forces try to enlarge it and produce another small eddy beside it. It can be seen that the oscillation frequency and amplitude increase to $f = 0.344$ and $A = 1.1103$, respectively. By comparing the flow conduct in Fig. 22 with that one in Fig. 21 as Reynolds number is kept constant at Re = 100, while Richardson number is decreased from Ri = 10 to 5, it is shown that the flow becomes more complicated. Thus, the weak flow-cell becomes stronger occupying the entire cavity, and changes into double adjacent flow-cells with the time. This can be attributed to the high conflict between the mechanical and buoyancy forces within the cavity area. The later case can be considered as a special case as the flow behaviour alters from a fully periodic flow into a quasi-periodic flow with a significant drop in the oscillation frequency from $f = 0.344$ to 0.0371, whereas the oscillation amplitude increases largely from $A = 1.1103$ to 2.092. In addition, by comparing the flow behaviour in Figs. 21 and 23 as Reynolds and Richardson numbers are remained constant at Re = 100 and Ri = 10, respectively, whereas the cavity depth increases from $H = -0.25$ into -1, it can be also seen that the flow becomes more intricate as the suppressed fluctuating vortex inside the shallow cavity transforms into a vigorous

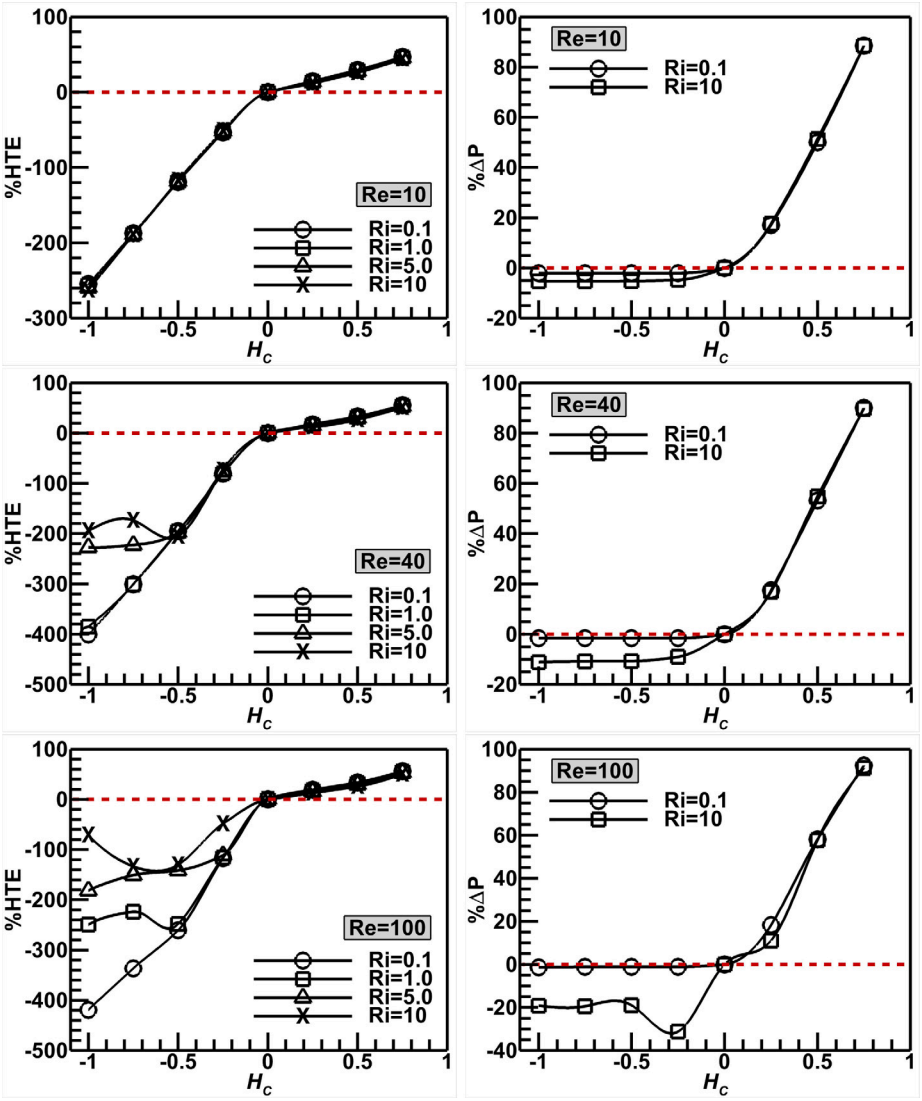

Fig. 16. (Left) Percent of Heat transfer enhancement and (Right) Percent of pressure drop, within the channel, when changing the cavity depth or the protrusion height, at different Richardson numbers (Ri = 0.1 – 10), and different Reynolds numbers (Re = 10 – 100).

dual flow cell system fluctuating inside the deep cavity. Consequently, the frequency and amplitude of the flow fluctuation are recorded to considerably increase from $f = 0.344$ to 0.404 and from $A = 1.1103$ to 1.5, respectively.

5. Conclusions

In the current study, numerical results for convective air-flow and heat transfer inside a horizontal plate-channel linked with an open-cavity or a protrusion containing a heat source on its entire horizontal lower surface, are presented. The attention is to investigate the effects of cavity depth and protrusion height on the heat transfer performance and pressure drop characteristics and compare their effects. According to the findings, the following conclusions could be drawn:

1. The intensity of recirculating flow inside the cavity or behind the protrusion regions increase as Reynolds number or Richardson number increases, resulting in a more effective cooling effect for all instances.

2. The existence of the protrusion affects the tendency of Nusselt number much highly than the presence of the cavity.

3. Interestingly, the presence of the cavity is found to reduce significantly the heat transfer from the heat source. Thus, as the cavity depth increases, the heat transfer augmentation decreases largely, and this negative effect becomes more pronounced at higher Reynolds numbers. However, in the protrusion case, the rate of heat transfer is found to increase substantially with increasing the protrusion height for all circumstances of Reynolds and Richardson numbers.

4. In the channel-cavity flow assembly, the pressure distribution along the channel is not influenced by the cavity height, except inside the cavity region. However, the increase in the protrusion height causes a significant increase in the pressure drop throughout the channel.

5. The effect of Reynolds number on Nusselt number in the cavity is trivial at low Richardson number, and becomes appreciable as Richardson number increases. Nevertheless, in the protrusion case, the effect of Reynolds number is significant and resulting in higher Nusselt numbers at larger protrusion heights.

6. The oscillatory flow transition is occurred only in the cavity case (inside the cavity containing the heat source), and the oscillation frequency and amplitude are found to increase by increasing Reynolds number, Richardson number, and/or the cavity depth.

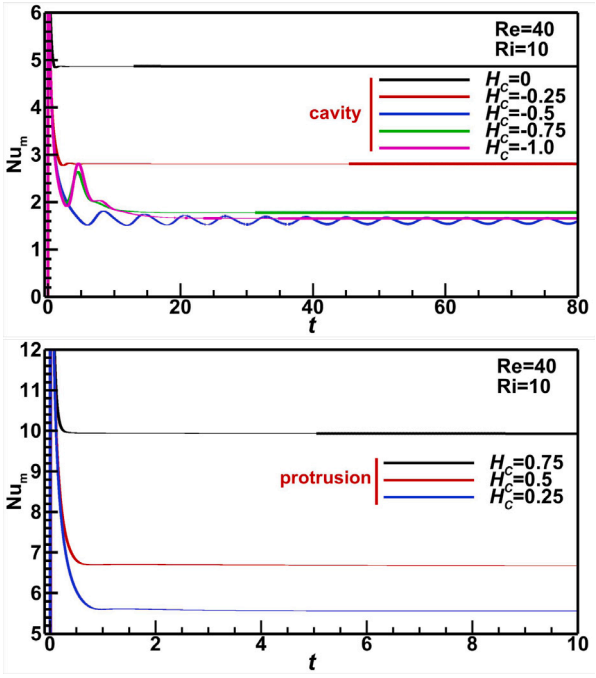

Fig. 17. Temporal variation of Nu_m for different H_c, at Re = 40 and Ri = 10.

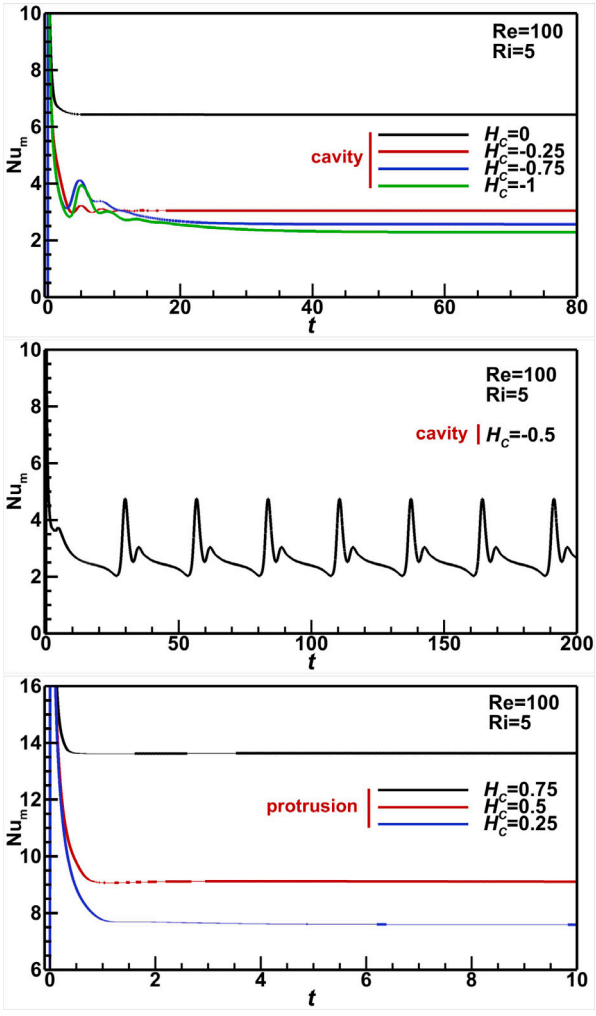

Fig. 18. Temporal variation of Nu_m for different H_c, at Re = 100 and Ri = 5.

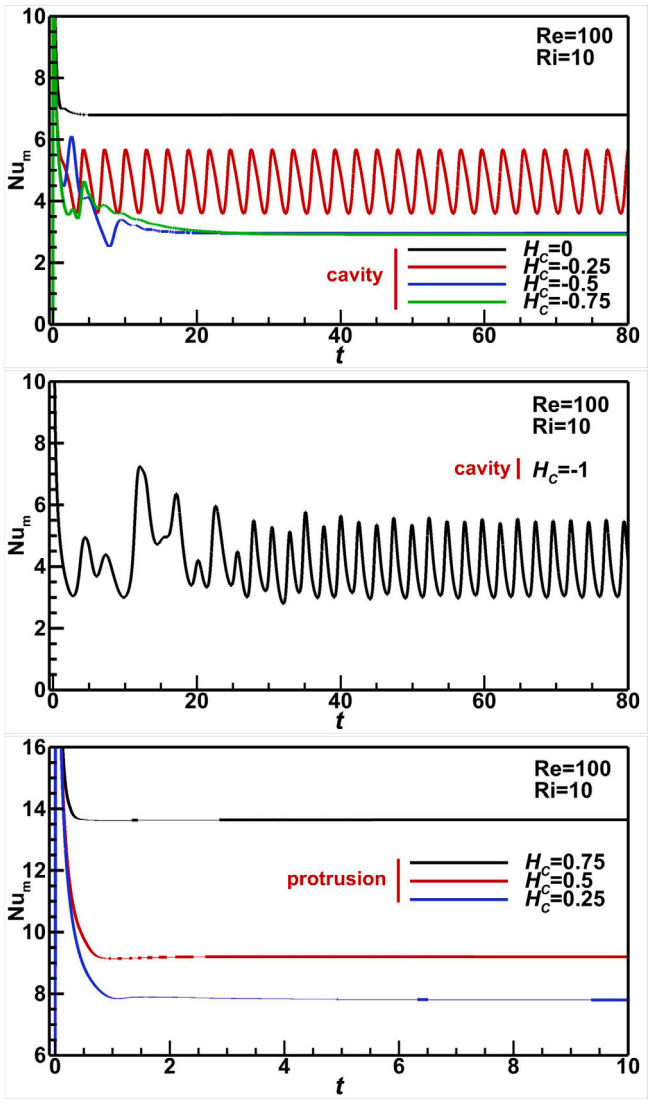

Fig. 19. Temporal variation of Nu_m for different H_c, at Re = 100 and Ri = 10.

CRediT authorship contribution statement

Amar S. Abdul-Zahra: Formal analysis, Data curation, Conceptualization. **Gazy F. Al-Sumaily:** Visualization, Methodology, Investigation. **Hasanen M. Hussen:** Writing – review & editing, Writing – original draft. **Mark C. Thompson:** Validation, Supervision, Software. **Hayder A. Dhahad:** Supervision, Resources, Project administration.

Funding

This research did not receive any specific grant from funding agencies in the public, commercial, or not-for-profit sectors.

Declaration of competing interest

The authors declare that they have no known competing financial interests or personal relationships that could have appeared to influence the work reported in this paper.

Acknowledgement

This research was supported in part by the Monash eResearch Centre and eSolutions-Research Support Services through the use of the MonARCH HPC Cluster.

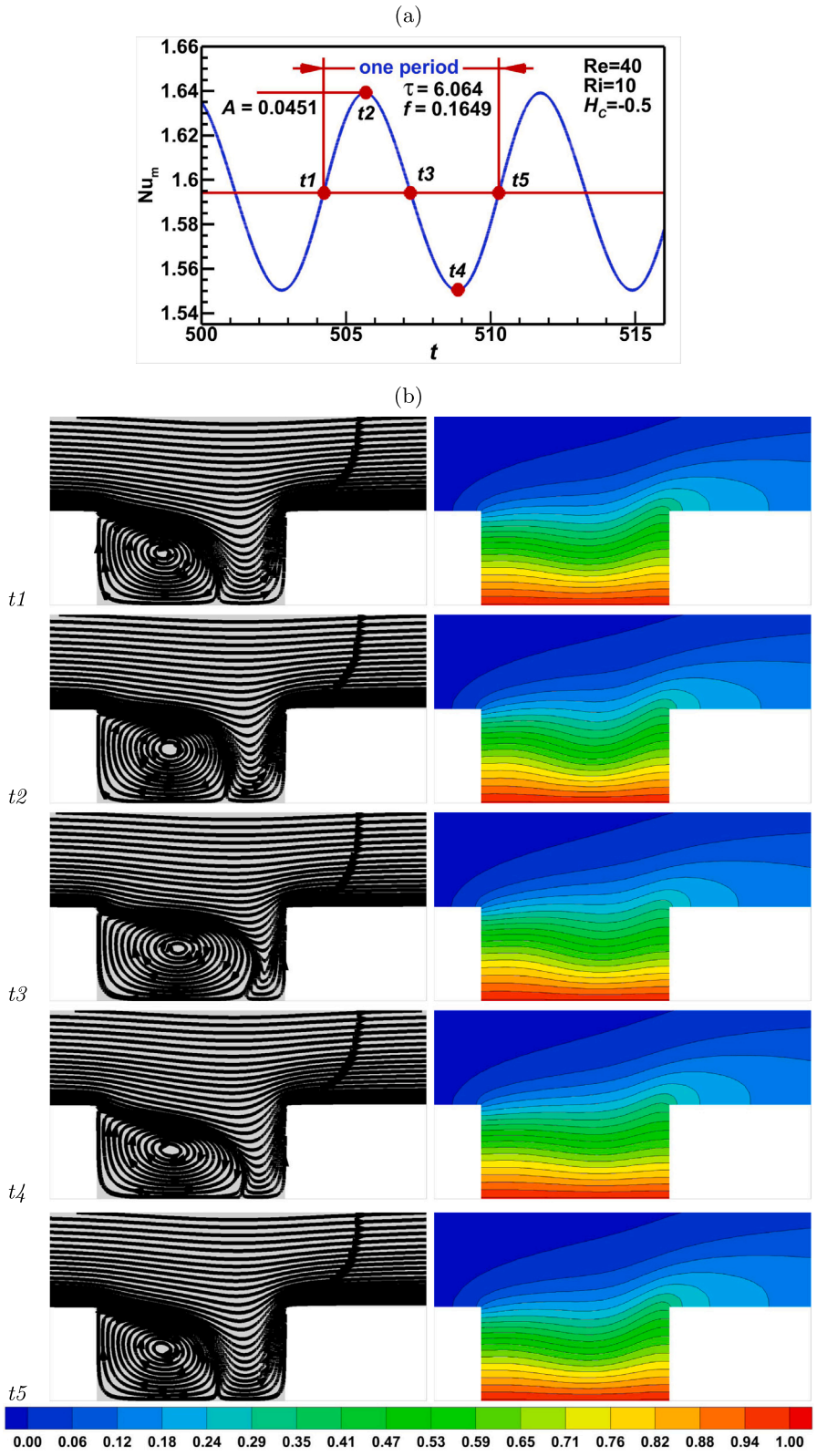

Fig. 20. (a) Temporal variation of Nu_m over one full period, (b) streamline and isotherm patterns at different certain times of the period, Re = 40, Ri = 10, and $H = -0.5$.

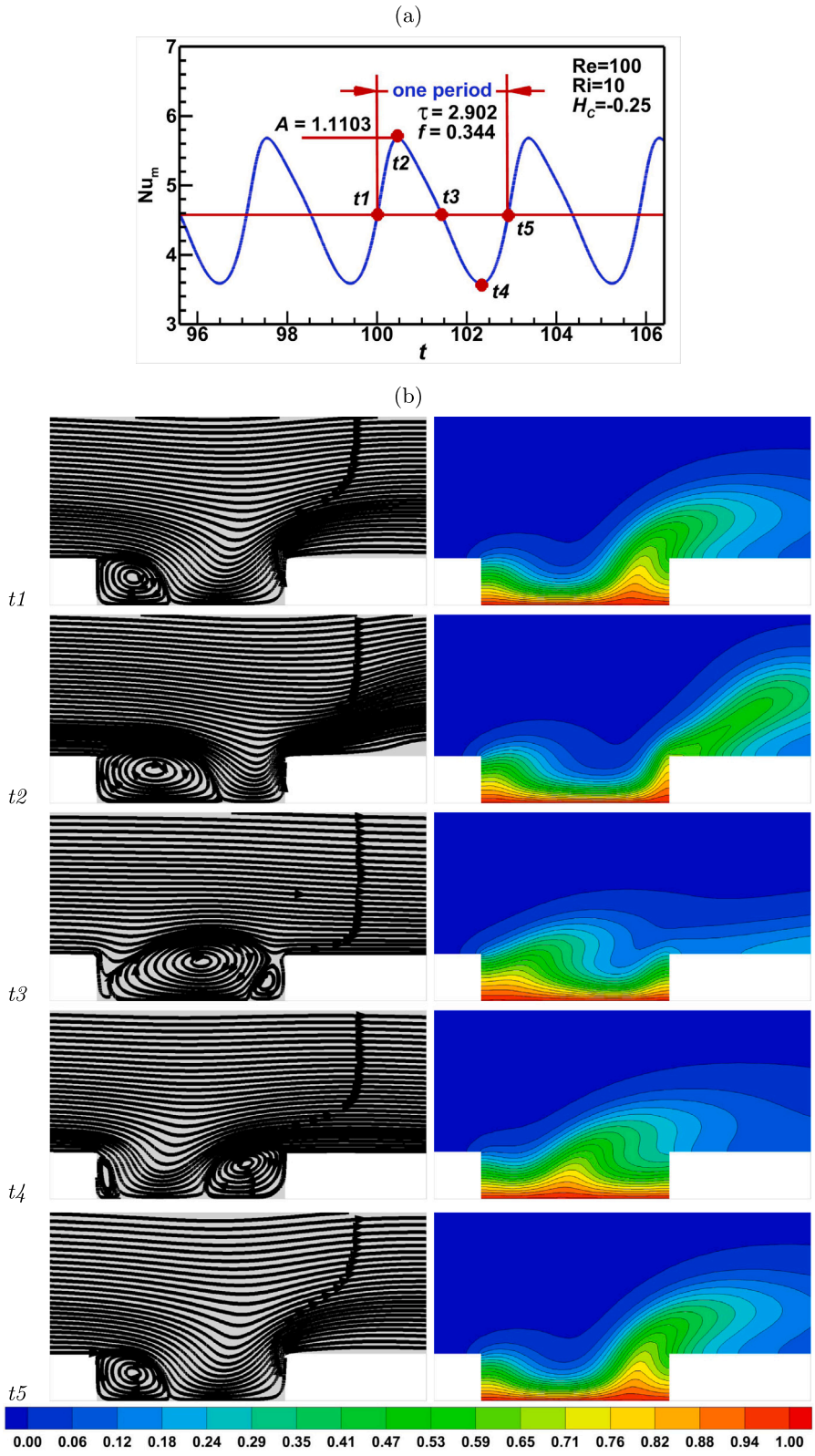

Fig. 21. (a) Temporal variation of Nu_m over one full period, (b) streamline and isotherm patterns at different certain times of the period, Re = 100, Ri = 10, and $H = -0.25$.

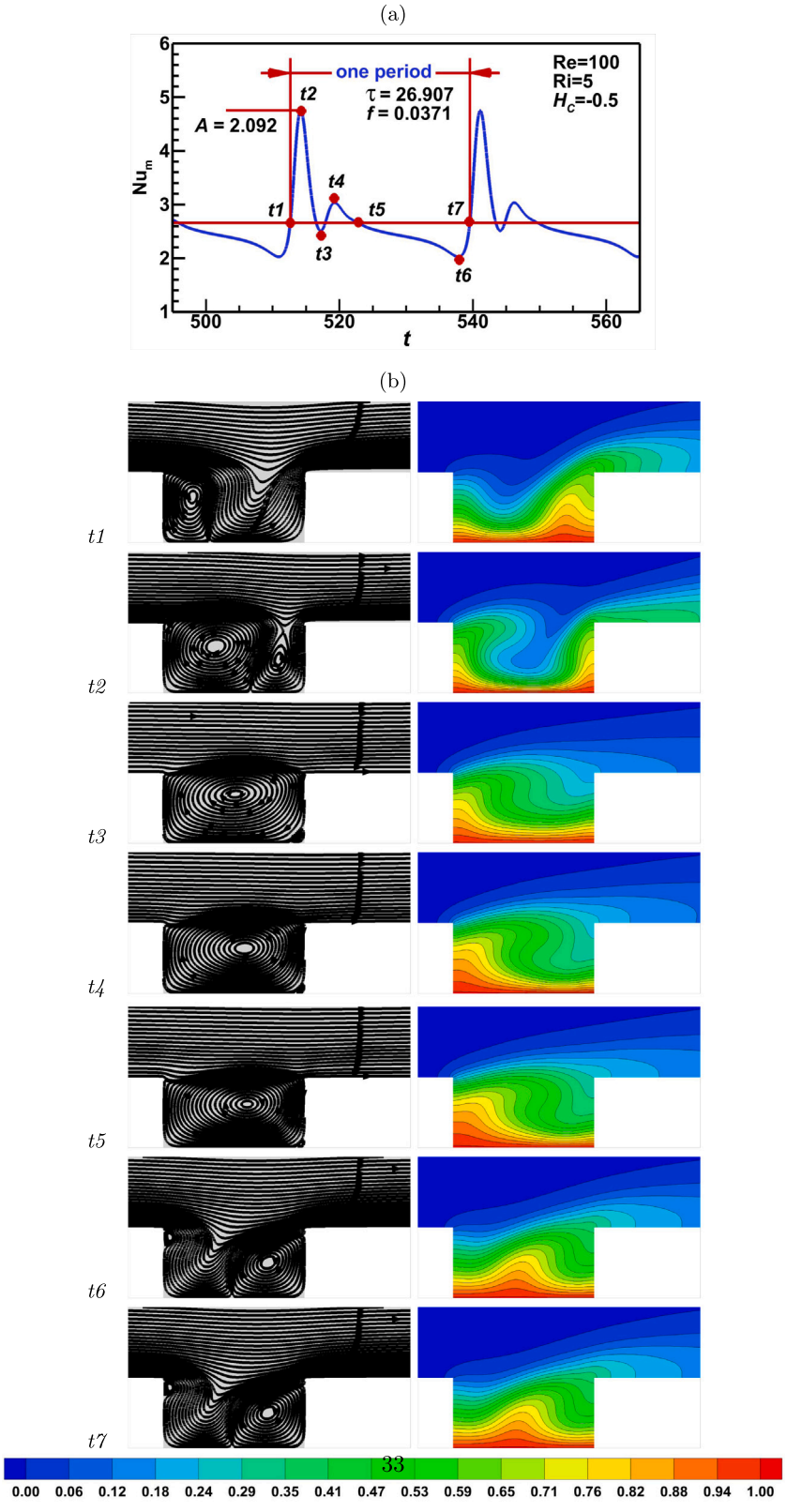

Fig. 22. (a) Temporal variation of Nu_m over one full period, (b) streamline and isotherm patterns at different certain times of the period, Re = 100, Ri = 5, and $H = -0.5$.

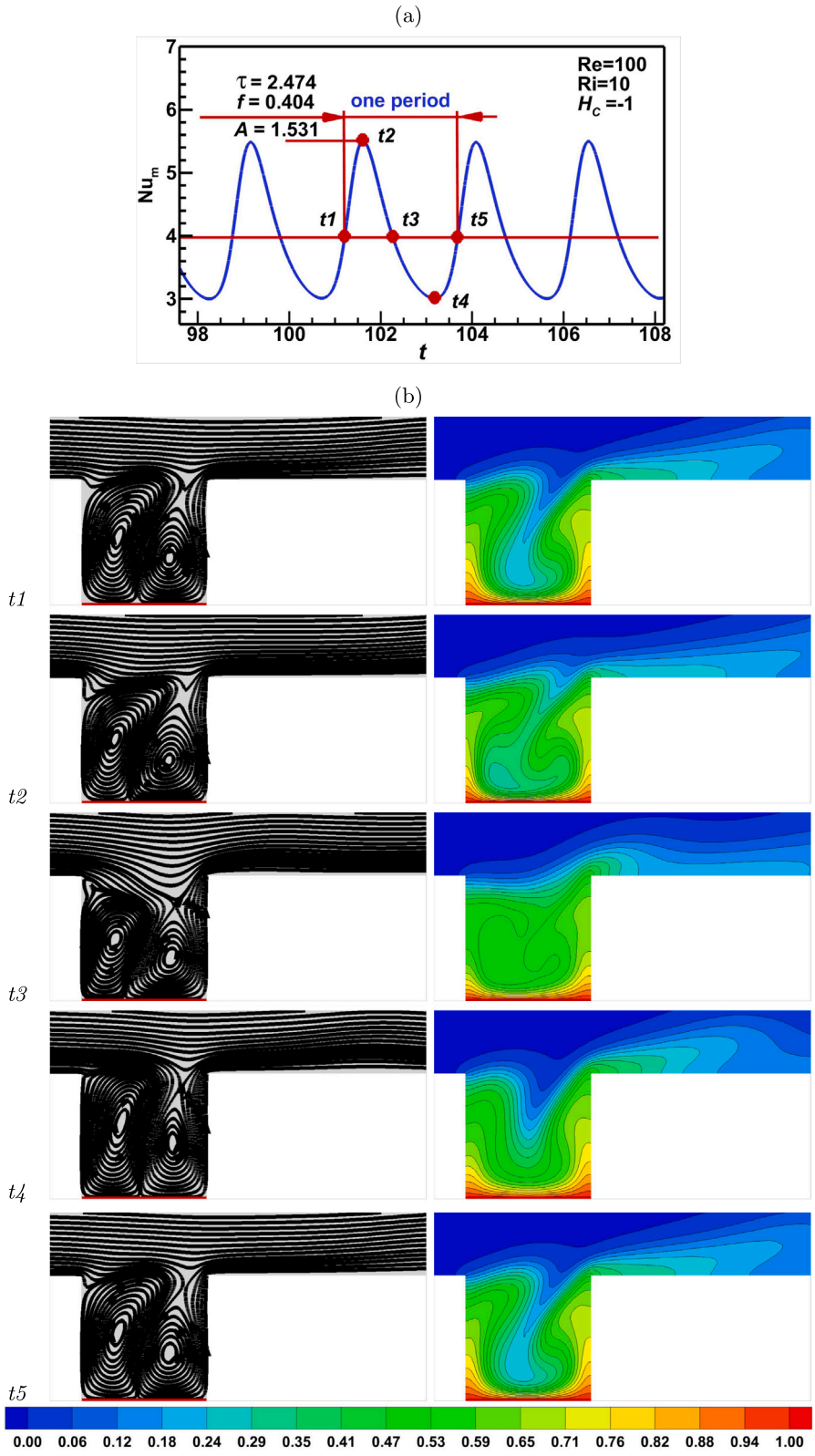

Fig. 23. (a) Temporal variation of Nu_m over one full period, (b) streamline and isotherm patterns at different certain times of the period, Re = 100, Ri = 10, and $H = -1$.

Data availability

Data will be made available on request.

References

[1] F.P. Incropera, Convection heat transfer in electronic equipment cooling, J. Heat Transf. 110 (1988) 1097–1111.
[2] G.P. Peterson, A. Ortega, Thermal control of electronic equipment and devices, Adv. Heat Transf. 20 (1990) 181–314.
[3] W.H. Alawee, G.F. Al-sumaily, H.A. Dhahad, M.C. Thompson, Numerical analysis of non-darcian mixed convection flows in a ventilated enclosure filled with a fluid-saturated porous medium, Therm. Sci. Eng. Prog. 24 (2021) 100922.
[4] S.A. Mohammed, G.F. Al-sumaily, H.A. Dhahad, M.C. Thompson, Heat transfer enhancement with pressure drop optimisation in a horizontal porous channel locally heated from below, Therm. Sci. Eng. Prog. 26 (2021) 101013.
[5] G.F. Al-Sumaily, H.A. Dhahad, M.C. Thompson, Mixed convection phenomenon in packed beds: A comprehensive review, Therm. Sci. Eng. Prog. 32 (2022) 101242.
[6] Y. Xuan, L. Qiang, Investigation on convective heat transfer and flow features of nanofluids, J. Heat Trans. ASME 125 (2003) 151–155.
[7] H. Heidary, M.J. Kermani, Effect of nano-particles on forced convection in sinusoidal-wall channel, Int. Commun. Heat Mass Transf. 37 (2010) 1520–1527.
[8] K. Khanafar, K. Vafai, A critical synthesis of thermophysical characteristics of nanofluids, Int. J. Heat Mass Transfer 54 (2011) 4410–4428.
[9] M. Rajarathinam, N. Nithyadevi, A.J. Chamkha, Heat transfer enhancement of mixed convection in an inclined porous cavity using Cu–water nanofluid, Adv. Powder Technol. 29 (2018) 590–605.
[10] M.S. Astanina, M.A. Sheremet, H.F. Oztop, N. Abu-Hamdeh, Mixed convection of al2o3-water nanofluid in a lid-driven cavity having two porous layers, Int. J. Heat Mass Transfer 118 (2018) 527–537.
[11] S.E. Ahmed, A.M. Aly, Mixed convection in a nanofluid-filled sloshing porous cavity including inner heated rose, J. Therm. Anal. Calorim. 143 (2021) 275–291.
[12] T. Naseem, U. Nazir, M. Sohail, H. Alrabaiah, E.M. Sherif, C. Park, Numerical exploration of thermal transport in water-based nanoparticles: A computational strategy, Case Stud. Therm. Eng. 27 (2021) 101334.
[13] N.S. Akbar, J. Akram, M.F. Hussain, E.N. Maraj, T. Muhammad, Thermal storage study and enhancement of heat transfer through hybrid jeffrey nanofluid flow in ducts under peristaltic motion with entropy generation, Therm. Sci. Eng. Prog. 49 (2024).
[14] F.A. Fethi Ahmet Çakmak, F. Selimefendigil, H.F. Öztop, A review on different nano-enhanced techniques for productivity improvement of solar stills, Therm. Sci. Eng. Prog. 55 (2024).
[15] A. Muhammad, U. Allauddin, A. Iranzo, Investigation of laminar flow and heat transfer performance of gallium alloy based nanofluids in minichannel heat sink, Therm. Sci. Eng. Prog. 56 (2024).
[16] T. Fusegi, Numerical study of convective heat transfer from periodic open cavities in a channel with oscillatory throughflow, Int. J. Heat Fluid Flow 18 (1997) 376–383.
[17] O. Manca, S. Nardini, K. Khanafer, K. Vafai, Effect of heated wall position on mixed convection in a channel with an open cavity, Numer. Heat Tr. A- APPL 43 (2003) 259–282.
[18] S.M. Aminossadati, B. Ghasemi, A numerical study of mixed convection in a horizontal channel with a discrete heat source in an open cavity, J. Mech. B/ Fluids 28 (2009) 590–598.
[19] N.M. Brown, F.C. Lai, Correlations for combined heat and mass transfer from an open cavity in a horizontal channel, Int. Commun. Heat Mass Transf. 32 (2005) 1000–1008.
[20] J.C. Leong, N.M. Brown, F.C. Lai, Mixed convection from an open cavity in a horizontal channel, Int. Commun. Heat Mass Transf. 32 (2005) 583–592.
[21] O. Manca, S. Nardini, K. Vafai, Experimental investigation of mixed convection in a channel with an open cavity, Exp. Heat Transf. 19 (2006) 53–62.
[22] W.A. Sabbar, M.A. Ismael, M. Almudhaffar, Fluid–structure interaction of mixed convection in a cavity-channel assembly of flexible wall, Int. J. Mech. Sci. 149 (2018) 73–83.
[23] F. Garcia, C. Trevino, J. Lizardi, L. Martinez-Suastegui, Numerical study of buoyancy and inclination effects on transient mixed convection in a channel with two facing cavities with discrete heating, Int. J. Mech. Sci. 155 (2019) 295–314.
[24] H. Laouira, F. Mebarek-Oudina, A.K. Hussein, L. Kolsi, A. Merah, O. Younis, Heat transfer inside a horizontal channel with an open trapezoidal enclosure subjected to a heat source of different lengths, Heat Transf. - Asian Res. 49 (2020) 406–423.
[25] L.R. Farhan, M.R. Asseel, A. Mohammed, A. Bagh, A.S. Nehad, D.C. Jae, Mixed convection in a horizontal channel-cavity arrangement with different heat source locations, Mathematics 11 (2023) article no. 1428.
[26] A. Firoozi, S. Majidi, M. Ameri, A numerical assessment on heat transfer and flow characteristics of nanofluid in tubes enhanced with a variety of dimple configurations, Therm. Sci. Eng. Prog. 19 (2024).
[27] I.M. Gazi, Z.S. Mounir, M.L. Phillip, Heat transfer in a channel with dimples and protrusions on opposite walls, J. Thermophys. Heat Trans. 15 (2001) 275–283.
[28] X. Yonghui, Z. Lu, Z. Di, X. Gongnan, Entropy generation and heat transfer performances of al2o3-water nanofluid transitional flow in rectangular channels with dimples and protrusions, Entropy 18 (2016) 148.
[29] M.K. Sahu, K.M. Pandey, S. Chatterjee, J. Chen, S. Shakya, S. Sahulhameedu, Numerical investigation of thermal-hydraulic performance of channel with protrusions by turbulent cross flow jet, in: AIP Conference Proceedings, Vol. 1966, 2018, 020021, 2018.
[30] M. Sobhani, A. Behzadmehr, Investigation of thermo-fluid behavior of mixed convection heat transfer of different dimples-protrusions wall patterns to heat transfer enhancement, Heat Mass Transf. 54 (2018) 3219–3229.
[31] B. Ebubekir, E. Bahadir, A. Murat, Y. Rumeysa, F. Kemal, P. Erhan, Cooling of heated blocks with triangular guide protrusions simulating printed circuit boards, Sustainability 14 (2022) 15856.
[32] R. Shaik, E. Punna, S.K. Gugulothu, Optimisation of thermohydraulic performance of triangular duct solar air heater with alternative dimple shaped protrusion and intrusion on the absorber plate, Therm. Sci. Eng. Prog. 42 (2024).
[33] G.F. Al-Sumaily, H.A. Dhahad, H.M. Hussen, M.C. Thompson, Influence of thermal buoyancy on vortex shedding behind a circular cylinder in parallel flow, Int. J. Therm. Sci 156 (2020) 106434.
[34] H.A. Dhahad, G.F. Al-Sumaily, W.H. Alawee, M.C. Thompson, Aiding and opposing re-circulating mixed convection flows in a square vented enclosure, Therm. Sci. Eng. Prog. 19 (2020) 100577.
[35] G.F. Al-Sumaily, H.M. Hussen, M.T. Chaichan, H.A. Dhahad, M.C. Thompson, Numerical analysis of flow shedding over an obstacle at low reynolds number, Int. J. Heat Fluid Flow 99 (2023) 109098.
[36] G. Abdelmassih, A. Vernet, J. Pallares, Steady and unsteady mixed convection flow in a cubical open cavity with the bottom wall heated, Int. J. Heat Mass Transfer 101 (2016) 682–691.
[37] A.J. Chorin, Numerical solution of the Navier–Stokes equations, Maths. Comput. 22 (1968) 745–762.
[38] G.E. Karniadakis, M. Israeli, S.A. Orszag, High-order splitting methods of the incompressible Navier–Stokes equations, J. Comput. Phys. 97 (1991) 414–443.
[39] F. Selimefendigil, Numerical analysis and POD based interpolation of mixed convection heat transfer in horizontal channel with cavity heated from below, Eng. Appl. Comput. Fluid Mech. 7 (2013) 261–271.